Applied Energy 162 (2016) 163–171

Contents lists available at ScienceDirect

Applied Energy

journal homepage: www.elsevier.com/locate/apenergy

Online state of charge estimation and open circuit voltage hysteresis modeling of $LiFePO_4$ battery using invariant imbedding method

Guangzhong Dong, Jingwen Wei, Chenbin Zhang, Zonghai Chen *

Department of Automation, University of Science and Technology of China, Hefei 230027, PR China

HIGHLIGHTS

- A novel online estimator for SOC and parameters is established using dual IIM.
- The OCV hysteresis phenomena is taken into account in the battery model.
- The observer for SOC estimation is designed against the effect of the hysteresis.
- The robustness of new method is validated under dynamic experimental conditions.

ARTICLE INFO

Article history:
Received 11 August 2015
Received in revised form 10 October 2015
Accepted 12 October 2015
Available online 11 November 2015

Keywords:
Lithium-ion battery
State-of-charge
Battery modeling
Invariant imbedding method
OCV hysteresis

ABSTRACT

The SOC (state-of-charge) of Li-ion (Lithium-ion) battery is an important evaluation index in BMS (battery management system) for EVs (Electric Vehicles) and smart grids. However, the existing special OCV (open circuit voltage) characteristics of $LiFePO_4$ batteries complicate the estimation of SOC. To improve the estimation accuracy and reliability for battery SOC and battery terminal voltage, an online estimation approach for SOC and parameters of a battery based on the IIM (invariant-imbedding-method) algorithm has been proposed. Firstly, by using the IIM algorithm, an online parameter identification method has been established to accurately capture the real-time characteristics of the battery, which include the OCV hysteresis phenomena. Secondly, a dual IIM algorithm is employed to develop a multi-state estimator for SOC of the battery. Note that the parameters of the battery model are updated with the real-time measurements of the battery current and voltage at each sampling interval. Finally, the proposed method has been verified by a $LiFePO_4$ battery cell under different operating current conditions. Experimental results indicate that the estimation value based on the proposed IIM-based estimator converges to real SOC with an error of $\pm 2\%$, and the battery model can simulate OCV hysteresis phenomena robustly with high accuracy.

1. Introduction

Effective electric energy storage is one of the most challenging issues for most of high electric power and energy consuming applications. In recent years, various electrochemical energy storage systems have been introduced for EVs (Electric Vehicles) and HEVs (Hybrid Electric Vehicles), like NiMH (Nickel/Metal Hydride), Li-ion (Lithium-ion) batteries as well as other types such as ultra-capacitors and fuel cells. State-of-the-art Li-ion (e.g., lithium–iron–phosphate, $LiFePO_4$) batteries offer the best trade-off between power/energy density and costs for energy storage in EVs and HEVs. They have been attracting special attention for their high power density, high energy density and long lifetime. For instance, Wang et al. [1] simulated the effects of a single battery cell inconsistency on the performance of a $LiFePO_4$ battery pack, and analyzed the relationship of the end-of-charge voltage with the ageing of a battery module to prevent battery cells being overcharged. Liu et al. [2] presented a new method based on the Back-Propagation Neural Network (BPNN) for the state of energy estimation of Li-ion battery. Among these lithium–iron–phosphate batteries, $LiFePO_4$ batteries are safer and cheaper than those based on lithium cobalt cathode and its evolutions. However, $LiFePO_4$ batteries are characterized by a lower operating voltage (2.0 – 3.65 V) and a flat OCV (open circuit voltage) with SOC (stage-of-charge) ranging from 20% to 80%. Moreover, they exhibit a pronounced hysteresis. As a critical aspect, these special OCV characteristics complicate the estimation of a battery's SOC [3].

For a reliable operation of EVs/HEVs, an effective BMS (battery management system) must evaluate the current amount of energy

* Corresponding author. Tel.: +86 055163606104.
E-mail address: chenzh@ustc.edu.cn (Z. Chen).

http://dx.doi.org/10.1016/j.apenergy.2015.10.092
0306-2619/

stored in the battery, its power capability and health, which demands online estimation of SOC and electric parameters of the battery. This task can only be achieved by means of an online estimator for battery SOC and parameters of battery model, where the hysteresis characteristics must be measured accurately and the hysteresis phenomenon must be described.

For accurate SOC estimation, many researches can be found in the literature, with the primary methods being the Ampere hour counting methods [4,5] and the electrical model based methods. The Ampere hour counting methods obtain SOC estimation through the accumulation of the battery current. This kind of methods is easy to implement, but it is an open-loop estimation so that its estimation accuracy can suffer from initial value errors and accumulated errors from incorrect measurements [6]. The electrical model based methods can overcome these drawbacks with varieties of electrical models to capture the relationship between SOC and the terminal voltage of the battery, then adaptive filter methods are applied for SOC estimation based on these battery models. These methods are closed-loop, and many algorithms such as EKF (extended Kalman filter) [7], UKF (unscented Kalman filter) [8], PF (particle filter) [9] and UPF (unscented particle filter) [10] are used in SOC estimation. These methods take SOC as a state variable, so they can solve the accumulated error of the Ampere hour counting methods by updating SOC based on the difference between the measured and the prediction value of the terminal voltage [2]. Some other works develop the artificial neural networks [11]. These approaches have been widely used in SOC estimation of Li-ion batteries, and most of them have achieved acceptable results. However, not all cells are created equal. The parameters of a battery model may be different between cells, and they may change during charging/discharging process. Therefore, it is important to estimate both SOC and the slowly time-varying cell parameters simultaneously [12]. To do this, Xiong et al. [13] proposed a data-driven parameter identification method through the RLS (recursive least square) algorithm, and the SOC is estimated based on adaptive EKF algorithm. It has disadvantage of that the RLS method is not appropriate when the system models are not linear in parameters. Liu et al. [14] built a dual-particle-filter estimator to obtain simultaneous SOC and drift current estimation based on a temperature-compensated model. However, it has not taken other battery parameters into account. Moreover, the OCV hysteresis phenomena should be considered for accurate battery modeling.

In terms of OCV hysteresis modeling, Dreyer et al. [15] presented a general explanation of the occurrence of inherent hysteretic behavior in insertion storage systems containing multiple particles. The proposed model also predicted the existence of apparent equilibria in battery electrodes the sequential particle-by-particle charging/discharging mechanism and the disappearance of two-phase behavior at special experimental conditions. Roscher et al. [16] pointed out how macroscopic effects, that was diffusion limitations, superimpose the interaction microscopic mechanisms and lead to a shrinkage of OCV hysteresis. In their following research [17], they derived a simple empiric models for the electric characteristics of Li-ion with emphasis on their specific OCV characteristics including hysteresis and special OCV recovery effects. Sasaki et al. [18] reported and characterized a memory effect in $LiFePO_4$. Its connection to the particle-by-particle charge/discharge model was also explained. Plett [19] established a zero-state order and widely used one-state order hysteresis model. Furthermore, Baronti et al. [3] gave an equivalent circuit model for the one-state hysteresis model, where the hysteresis parameter was calculated as a fitting parameter by minimizing the RMSE (Root Mean Square Error) between the simulation results and the experimental ones. It was an off-line method. And the identification problem of the unknown hysteresis parameter required the processing of large quantities of data.

In this paper, in order to accurately estimate SOC and model hysteresis phenomena, an online estimation approach for SOC and parameters of the battery based on IIM (invariant-imbedding-method) algorithm has been carried out. In the proposed method, one IIM algorithm is employed to develop an online parameter identification method through the real-time measurements of battery currents and voltages. In addition, the other IIM algorithm is applied to establish SOC estimator against the effect of the hysteresis phenomenon and noises interference caused by incorrect measurements of voltages and currents. This approach has the potential to eliminate the drawback of parameter variation and reduce the influence from different operating conditions. What is more, the performance of this estimator has been verified and evaluated by $LiFePO_4$ cells.

The remainder of the paper is organized as follows: The test bench and some experimental tests on an IFP1865140-type battery, including OCV test and internal resistance test are described in Section 2. Section 3 gives the lumped parameter batter model and the implement flowchart of the parametric modeling approach. Section 4 presents a review of the proposed dual IIM algorithm, and then gives the online estimation approach implement flowchart of battery SOC. The experiment, simulation results and evaluation of the proposed method are reported in Section 5. Finally, Section 6 gives some conclusions and final remarks.

2. Experimental

2.1. Test bench

The experimental setup is shown in Fig. 1. It consists of (1) $LiFePO_4$ test batteries; (2) a programmable supply (Chroma 626006-30V-80A), (3) a programmable electric load for discharging (Chroma 63640-80V-80A); and (4) a host computer for online experiment control as well as battery voltage and current recording with a period of 1 s; the Chroma 626006-30V-80A is used to charge the battery with a maximum voltage of 30 V and a maximum current of 100 A. The Chroma 63640-80V-80A is used to load the battery with a maximum voltage 80 V and a maximum current of 80 A. The experimental data such as current, voltage, accumulative ampere-hours (A h) are measured by the supply as well as the load and recorded by the host computer. The experimental results are stored on a PC, and used as inputs for MATLAB. All experiments

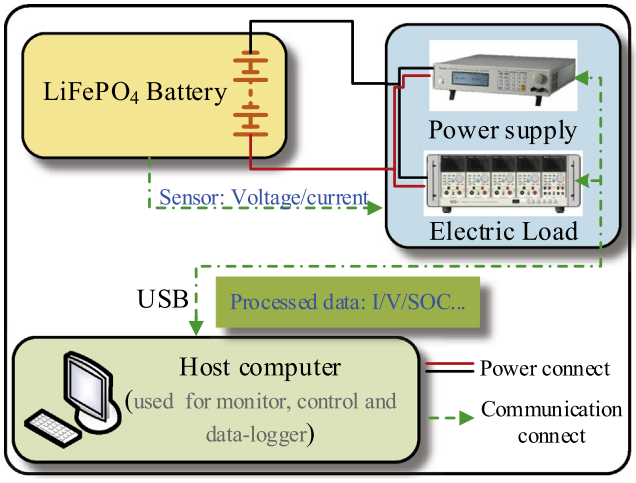

Fig. 1. Configuration of the battery test bench.

were performed at room temperature (25–30 °C). Parameters of the test batteries are given in Table 1.

2.2. OCV test

In order to investigate the relationship between OCV and SOC, a test is performed on $LiFePO_4$ batteries. Its test method is similar with Baronti et al. [3]. SOC is changed with charge/discharge steps. The variation (ΔSOC) of the charge stored in the cell is 5% of the total available capacity in each step. To do so, a current pulse of 0.5 h duration and amplitude equal to C/10 is used. Each charge/discharge is followed by an 1 h rest of the cell, presented by the block of 1 h rest in the flow diagram of Fig. 2 with the aim to extract the proper OCV value at the given SOC in steady-state conditions. OCV is thus defined as the cell voltage at the end of the 1 h rest. The OCV values after charge/discharge are denoted as OCV_{up} and OCV_{lw}, respectively. Then, the average value of OCV_{up} and OCV_{lw} is defined as $U_{oc}(z)$, as shown in Eq. (1). Additionally, it is possible to define hysteresis voltage – U_H as a function of the SOC history. Here, the maximum hysteresis loop which contains every evolution and thus trajectory in the plane SOC – U_H is introduced. The maximum hysteresis loop is calculated from its upper bound OCV_{up} and lower bound OCV_{lw}. It is useful to define the non-negative function $M_d(z)$ representing the maximum deviation due to the hysteresis of the OCV value. The $M_d(z)$ is defined as Eq. (2).

$$U_{oc}(z) = (OCV_{up}(z) + OCV_{lw}(z))/2 \tag{1}$$

$$M_d(z) = (OCV_{up}(z) - OCV_{lw}(z))/2 \tag{2}$$

The experimental results of OCV test are shown in Fig. 3. Fig. 3 (a) shows that the OCV drops quickly as SOC approaches 0% and rises quickly as SOC reaches around 100%. In a relative large transitional portion of SOC, the characteristic is rather flat, with two particularly flat zones in the upper and in the lower parts of the curve. The first flat zone is around SOC = 50%, and the second one is around SOC = 85%. The hysteresis effect between the discharge and the charge curves can be noted. The hysteresis major loop indicates the experimental points obtained after 1 h relaxation time. Finally, the maximum deviation $M_d(z)$ due to the hysteresis of the OCV value is plotted in Fig. 3(b). The OCV deviation is less than 36.3 mV all-over the entire SOC range.

Table 1
Parameters of a $LiFePO_4$ cell.

Model	GX IFP1865140
Nominal capacity	10 Ah
Nominal voltage	3.3 V
Charging/discharging cut-off voltage	3.65 V/2.0 V
Maximum continues charge current	10 A
Maximum continues discharge current	20 A
Operation temperature (charge/discharge)	−10 °C ~ 45 °C −20 °C ~ 60 °C
Weight	330 ± 10 g
Size (length/width/height)	140/65/18 mm

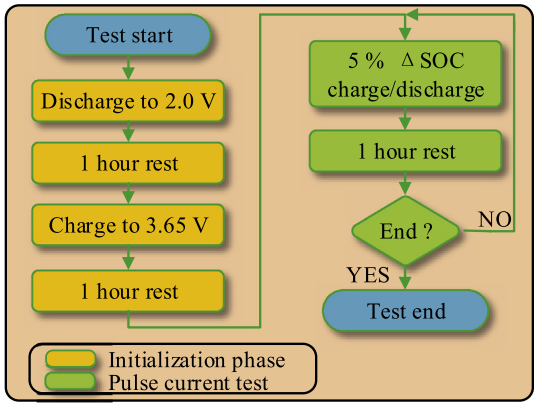

Fig. 2. Flow chart of an OCV test execution.

2.3. Internal resistance test

The ohmic inner resistance and DCIR (direct current internal resistance) $\{R_o, R_{dc}\}$ are measured by the methods mentioned in [20]. To obtain the lamped resistance, the pulse current with 10 s duration is applied to the batteries. As shown in Fig. 4(a). The lumped resistance is derived as Eq. (3) in accordance with Ohm's law. Corresponding test profile is shown in Fig. 4(b). Then, the $\Delta U_{dc}/\Delta U_o - I$ curves can be obtained at each certain SOC. Finally, the slopes of the $\Delta U_o/\Delta U_{dc} - I$ are $\{R_o, R_{dc}\}$, respectively.

$$\begin{aligned} R_o &= \Delta U_o/I = (|U_o - U_s|)/I \\ R_{dc} &= \Delta U_{dc}/I = (|U_{dc} - U_s|)/I \end{aligned} \tag{3}$$

The experimental results of internal resistance test are plotted in Fig. 5. First, $\{R_o, R_{dc}\}$ at charge and discharge are regarded as the slopes of $\Delta U_o/\Delta U_{dc} - I$, as shown in Fig. 5(a). The resistance values at different SOC are plotted in Fig. 5(b). According to Fig. 5(b), $\{R_o, R_{dc}\}$ may be change along with SOC. On the other hand, they

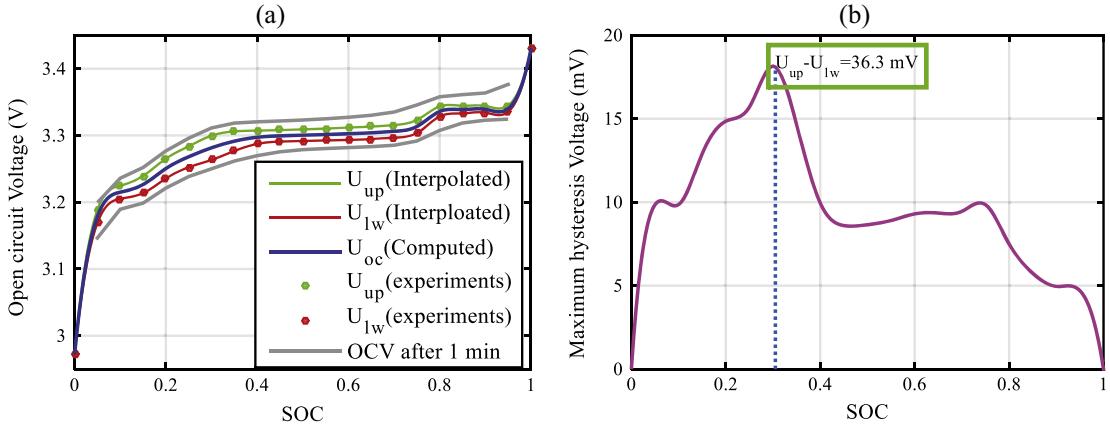

Fig. 3. Test results of OCV test: (a) hysteresis major loop and average OCV, and (b) maximum positive hysteresis.

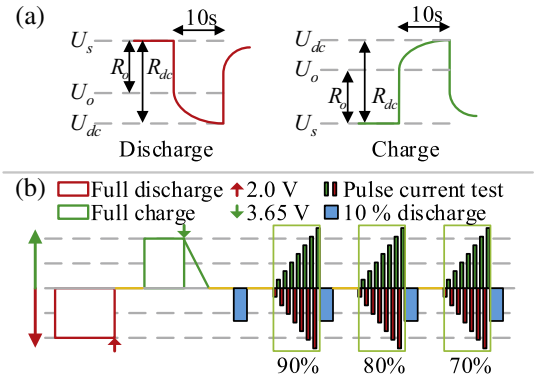

Fig. 4. Internal resistance measurement and test profile: (a) measurement, and (b) test profile.

may change along with different operating conditions. Therefore, these parameters must be identified online to obtain accurate battery model.

3. Parametric model approach

3.1. Battery model

A common definition of SOC is formulated as:

$$\mathrm{SOC}(t) = \mathrm{SOC}(t_0) - \int_{t_0}^{t} I_L(\tau)/C_n \mathrm{d}\tau \tag{4}$$

Based on Eq. (4), the discrete-time recurrence may then be written as:

$$z_k = z_{k-1} - I_{L,k-1}\Delta t/C_N \tag{5}$$

where z denotes the SOC of the battery, z_k and z_{k-1} denote SOC at sampling time k and $k-1$, respectively. $I_{L,k}$ represents the load current of the battery at time k. Δt is sampling time. C_N denotes the maximum available capacity of the battery.

An accurate battery model that can simulate the dynamic behavior of Li-ion batteries is essential to SOC estimation. Therefore, many battery models have been proposed, among which the most commonly used are the equivalent circuit models, including the first-order resistor–capacitor (RC) model, the second-order RC model and the complicated RC model. In consideration of hysteresis phenomenon, the second-order RC models are attracting more attentions, such as Petzl and Danzer [21]. Therefore, this paper uses

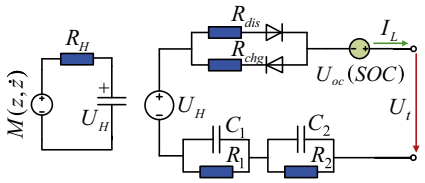

Fig. 6. The schematic diagram of second order equivalent circuit battery model.

two RC networks based self-correct equivalent circuit model to describe the dynamics of a battery. The model can be divided into four parts: The first part is the voltage source, OCV (open-circuit voltage) – U_{oc}; the second is the rapidly changed voltage part – herein we use a resistor R_o including R_{dis} at discharge and R_{chg} at charge to describe it; the third is the dynamic voltage performances – $U_{RC_i}(i = 1, 2)$, which are terms that account for relaxation phenomena occurring also when $I_L = 0$; the last part is the hysteresis term U_H. The schematic diagram of the model is shown in Fig. 6.

Where I_L is the load current and U_t is the terminal voltage. $M(z, \dot{z}) = \mathrm{sgn}(\dot{z})M_d(z)$. The OCV function $U_{oc}(z)$ is expressed as follows:

$$U_{oc}(z) = K_0 + K_1 z + K_2 z^2 + K_3/z + K_4 \ln(z) + K_5 \ln(1-z) \tag{6}$$

where z is the abbreviation of SOC. $K_i(i = 0, 1, \ldots, 5)$ are six polynomial coefficients of the model.

The electrical behavior of the second-order RC model can be expressed as:

$$\dot{U}_i = -U_i/R_iC_i + I_L/C_i \tag{7}$$

$$U_t = U_{oc} - U_1 - U_2 - I_L R_o \tag{8}$$

where $U_i, i = 1, 2$ is the terminal voltage of the ith RC network.

As to hysteresis voltage U_H, the differential equations describing the model in the SOC – U_H plane can be written as:

$$dU_H/dz = -\gamma \mathrm{sign}(\dot{z})U_H + \gamma M_d(z) \tag{9}$$

where $1/\gamma$ is a sort of charge constant analogous to the time constant used in the time domain. The hysteresis voltage U_H can be calculated by solving Eq. (9):

$$dU_H/dt = -U_H/\tau_H + M_d(z)/\tau_H \tag{10}$$

where $\tau_H = R_H C_H$, $C_H = 1F$ and $R_H = C_n/\gamma|I_L|$. Eq. (10) may be converted into a difference equation for discrete-time application as:

$$U_{H,k+1} = T(I_{L,k})U_{H,k} + (1 - T(I_{L,k}))M(z, \dot{z}) \tag{11}$$

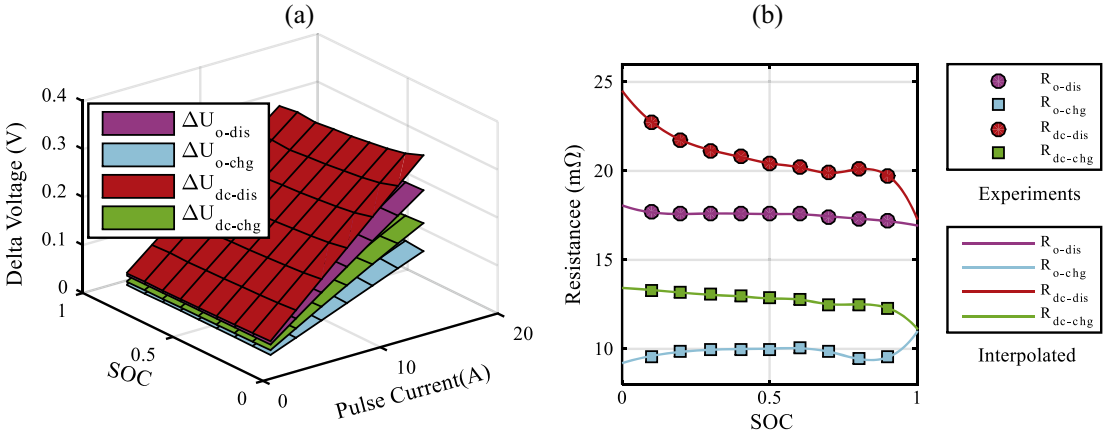

Fig. 5. The internal resistance test results: (a) experimental points of ΔU_o, ΔU_{dc}, and (b) resistance values at different SOC.

where $T(I_{L,k}) = \exp(-\gamma|I_{L,k}|\Delta t/C_n)$.

3.2. Parameter identification approach

The state equation of the lumped parameter battery model described in Eqs. (7) and (8) can be discretized with a linear discrete form,

$$\begin{cases} U_{i,k+1} = e^{-\frac{\Delta t}{R_i C_i}} U_{i,k} + \left(1 - e^{-\frac{\Delta t}{R_i C_i}}\right) R_i I_{L,k} \\ U_{t,k} = U_{oc,k} - U_{1,k} - U_{2,k} - I_{L,k} R_o \end{cases} \tag{12}$$

Defining $\alpha_i = \exp(-\Delta t/R_i C_i)$ and $\Gamma_k = T(I_{L,k}) = \exp(-\gamma|I_{L,k}|\Delta t/C_n)$, Combine Eqs. (4), (11) and (12), the system state-space equation can be achieved by

$$\begin{cases} \mathbf{x}_{k+1} = f(\mathbf{x}_k, \mathbf{u}_k, \boldsymbol{\theta}_k) + \mathbf{w}_k \\ y_k = g(\mathbf{x}_k, \mathbf{u}_k, \boldsymbol{\theta}_k) + v_k \end{cases}$$
$$\Updownarrow$$
$$\begin{cases} \begin{pmatrix} z_{k+1} \\ U_{1,k+1} \\ U_{2,k+1} \\ U_{H,k+1} \end{pmatrix} = \begin{pmatrix} 1 & 0 & 0 & 0 \\ 0 & \alpha_1 & 0 & 0 \\ 0 & 0 & \alpha_2 & 0 \\ 0 & 0 & 0 & \Gamma_k \end{pmatrix} \begin{pmatrix} z_k \\ U_{1,k} \\ U_{2,k} \\ U_{H,k} \end{pmatrix} + \begin{pmatrix} -\Delta t/C_N & 0 \\ (1-\alpha_1)R_1 & 0 \\ (1-\alpha_2)R_2 & 0 \\ 0 & 1-\Gamma_k \end{pmatrix} \\ \quad \times \begin{pmatrix} I_{L,k} \\ M(z,\dot{z}) \end{pmatrix} + \mathbf{w}_k \\ U_{t,k} = U_{oc,k} - U_{1,k} - U_{2,k} - I_{L,k} R_o + U_{H,k} + v_k \end{cases} \tag{13}$$

where $\mathbf{x}_k$ is the state vector at discrete-time index k. $f(\cdot)$ and $g(\cdot)$ are state transition and measurement functions, respectively. The vector $\mathbf{u}_k$ is the measured exogenous system input at sampling time k and $\mathbf{w}_k$ is the process noise with known pdfs: $\mathbf{w}_k \sim N(0, \mathbf{Q}_k)$ and is used to account for current-sensor error and inaccuracy of the state equation. y_k represents system output and $\mathbf{v}_k$ is the measurement noise with known pdfs: $\mathbf{v}_k \sim N(0, \boldsymbol{\Lambda}_k)$, which is used to account for voltage sensor error and inaccuracy of the output equation. $\boldsymbol{\theta}_k$ denotes the battery model parameters, as shown in Eq. (14).

$$\boldsymbol{\theta}_k = [R_{dis},\ R_{chg},\ \alpha_1,\ \alpha_2,\ R_1,\ R_2,\ \gamma]^T \tag{14}$$

In this study, these parameters are identified online based on the IIM algorithm. To do so, a state-space model which describes the dynamics of the parameters $\boldsymbol{\theta}$ of the system model is required. In electro-chemical cells, the true parameters will change only very slowly [12], so we model them as constant with some small perturbation, as shown in Eq. (15).

$$\hat{\boldsymbol{\theta}}_{k+1} = \hat{\boldsymbol{\theta}}_k + \mathbf{r}_k \tag{15}$$

where $\hat{\boldsymbol{\theta}}_k$ is the estimation of parameters matrix at sample time k. $\mathbf{r}_k$ is a fictitious small white noise input. The output equation required for IIM based system identification must be a measurable function of the system parameters. Herein, we use

$$d_k = g(\mathbf{x}_k, \mathbf{u}_k, \boldsymbol{\theta}_k) + n_k \tag{16}$$

where n_k models the sensor noises and modeling error. This state-space model and cell data are used to estimate the system parameters based on IIM algorithm.

4. Algorithm implementation

To make the state estimator more concrete, discrete time state-space model is used to describe the system. Then a dual IIM algorithm is established to develop an online state and parameter estimation method. IIM is one of the direct methods in the studies, such as Sridhar [22] and Akin-Bohner and Atici [23], which focus on state and parameter estimation in noisy nonlinear systems. However, the joint estimation method for state and parameters in these researches is to augment the model state vector with the model parameters and simultaneously estimate the values of this augmented state vector. It has the disadvantage of large matrix operations due to the high dimensionality of the resulting augmented model. The dual IIM algorithm used here uses two separate IIM for state estimation and parameter estimation, where the matrix operations are simpler. The specific algorithm is described in Table 2. The flowchart of the model based multi-state joint estimator with IIM based dual filters can be viewed by drawing a block diagram as in Fig. 7.

Based on the nonlinear state-space models, the relevant matrixes for dual IIM estimator can be deduced, and the state – $\mathbf{x}_k$, output – y_k, input – $\mathbf{u}_k$, $\mathbf{A}_k$ and $\mathbf{C}_k^x$ are shown in Eq. (27).

$$\begin{cases} \mathbf{x}_k = (\,z_k \quad U_{1,k} \quad U_{2,k} \quad U_{H,k}\,);\ y_k = U_{t,k};\ \mathbf{u}_k = \begin{pmatrix} I_{L,k} & M(z,\dot{z}) \end{pmatrix}^T; \\ \mathbf{A}_k = \begin{pmatrix} 1 & 0 & 0 & 0 \\ 0 & \alpha_1 & 0 & 0 \\ 0 & 0 & \alpha_2 & 0 \\ 0 & 0 & 0 & \Gamma_k \end{pmatrix};\ (\mathbf{C}_k^x)^T = \begin{pmatrix} \frac{\partial U_{oc,k}}{\partial z}\big|_{z=z_k} \\ -1 \\ -1 \\ 1 \end{pmatrix} \end{cases} \tag{27}$$

As to $\mathbf{C}_k^\theta$, it can be expressed as the following three total derivatives. These three total derivatives can be computed recursively, initialized with zero values.

$$\frac{dg(\hat{\mathbf{x}}_k^-, u_k, \boldsymbol{\theta})}{d\boldsymbol{\theta}} = \frac{\partial g(\hat{\mathbf{x}}_k^-, u_k, \boldsymbol{\theta})}{\partial \boldsymbol{\theta}} + \frac{\partial g(\hat{\mathbf{x}}_k^-, u_k, \boldsymbol{\theta})}{\partial \hat{\mathbf{x}}_k^-} \frac{d\hat{\mathbf{x}}_k^-}{d\boldsymbol{\theta}} \tag{28}$$

$$\frac{d\hat{\mathbf{x}}_k^-}{d\boldsymbol{\theta}} = \frac{\partial f(\hat{\mathbf{x}}_{k-1}^+, u_{k-1}, \boldsymbol{\theta})}{\partial \boldsymbol{\theta}} + \frac{\partial f(\hat{\mathbf{x}}_{k-1}^+, u_{k-1}, \boldsymbol{\theta})}{\partial \hat{\mathbf{x}}_{k-1}^+} \frac{d\hat{\mathbf{x}}_{k-1}^+}{d\boldsymbol{\theta}} \tag{29}$$

Table 2
Summary of dual IIM algorithm for state and parameter estimation.

The nonlinear state-space models

$$\begin{cases} \hat{\boldsymbol{\theta}}_{k+1} = \hat{\boldsymbol{\theta}}_k + \mathbf{r}_k \\ d_k = g(\mathbf{x}_k, u_k, \boldsymbol{\theta}_k) + e_k \end{cases} \text{ and } \begin{cases} \mathbf{x}_{k+1} = f(\mathbf{x}_k, \mathbf{u}_k, \boldsymbol{\theta}_k) + \mathbf{w}_k \\ y_k = g(\mathbf{x}_k, \mathbf{u}_k, \boldsymbol{\theta}_k) + v_k \end{cases} \tag{17}$$

Step 1 Initialization: For $k = 0$, set

(a) $\hat{\boldsymbol{\theta}}_0^+ = E[\boldsymbol{\theta}_0], \boldsymbol{\Sigma}_{\theta,0}^+ = E\left[(\boldsymbol{\theta}_0 - \hat{\boldsymbol{\theta}}_0^+)(\boldsymbol{\theta}_0 - \hat{\boldsymbol{\theta}}_0^+)^T\right]$

(b) $\hat{\mathbf{x}}_0^+ = E[\mathbf{X}_0],\ \boldsymbol{\Sigma}_{x,0}^+ = E[(\mathbf{x}_0 - \hat{\mathbf{x}}_0^+)(\mathbf{x}_0 - \hat{\mathbf{x}}_0^+)^T]$

Step 2 Computation: For $k = 1, 2, \ldots$, compute:

(a) Time update:

Time update for parameter estimator: (18)

$\hat{\boldsymbol{\theta}}_k^- = \hat{\boldsymbol{\theta}}_{k-1}^+,\ \boldsymbol{\Sigma}_{\theta,k}^- = \boldsymbol{\Sigma}_{\theta,k-1}^+ + \boldsymbol{\Sigma}_r$

Time update for SOC estimator: (19)

$\hat{\mathbf{x}}_k^- = f(\hat{\mathbf{x}}_{k-1}^+, \mathbf{u}_{k-1}, \hat{\boldsymbol{\theta}}_k^-),\ \boldsymbol{\Sigma}_{x,k}^- = \mathbf{A}_{k-1}\boldsymbol{\Sigma}_{x,k-1}^+\mathbf{A}_{k-1}^T + \boldsymbol{\Sigma}_w$

(b) Error innovation:

Prediction error: $e_k = y_k - \hat{y}_k = y_k - g\left(\hat{\mathbf{x}}_k^-,\ \mathbf{u}_k, \hat{\theta}_k^-\right)$ (20)

Error matrix: $\mathbf{E}_k^x = (\mathbf{C}_k^x)^T\boldsymbol{\Sigma}_v^{-1}e_k;\ \mathbf{E}_k^\theta = (\mathbf{C}_k^\theta)^T\boldsymbol{\Sigma}_r^{-1}e_k$ (21)

Partial derivative of the error matrix: (22)

$\partial\mathbf{E}_k^x/\partial\hat{\mathbf{x}}_k^- = -(\mathbf{C}_k^x)^T\boldsymbol{\Sigma}_v^{-1}\mathbf{C}_k^x;\ d\mathbf{E}_k^\theta/d\hat{\boldsymbol{\theta}}_k^- = -(\mathbf{C}_k^\theta)^T\boldsymbol{\Sigma}_r^{-1}\mathbf{C}_k^\theta$

(c) Measurement update:

Measurement for SOC estimator:

Error covariance measurement update: (23)

$\boldsymbol{\Sigma}_{x,k}^+ = \boldsymbol{\Sigma}_{x,k}^-[\mathbf{I} - \partial\mathbf{E}_k/\partial\hat{\mathbf{x}}_k^-\boldsymbol{\Sigma}_{x,k}^-]^{-1}$

Measurement for SOC estimator: $\hat{\mathbf{x}}_k^+ = \hat{\mathbf{x}}_k^- + \boldsymbol{\Sigma}_{x,k}^+\mathbf{E}_k$ (24)

Error covariance measurement update: (25)

$\boldsymbol{\Sigma}_{\theta,k}^+ = \boldsymbol{\Sigma}_{\theta,k}^-\left[\mathbf{I} - \partial\mathbf{E}_k^\theta/\partial\hat{\mathbf{x}}_k^-\boldsymbol{\Sigma}_{\theta,k}^-\right]^{-1}$

Parameter estimate measurement update: (26)

$\hat{\boldsymbol{\theta}}_k^+ = \hat{\boldsymbol{\theta}}_k^- + \boldsymbol{\Sigma}_{\theta,k}^+\mathbf{E}_k^\theta$

Where $\mathbf{C}_k^\theta = \frac{dg(\hat{\mathbf{x}}_k^-, u_k, \boldsymbol{\theta})}{d\boldsymbol{\theta}}\Big|_{\boldsymbol{\theta}=\hat{\boldsymbol{\theta}}_k^-}$, $\mathbf{C}_k^x = \frac{\partial g(\mathbf{x}_k, u_k, \hat{\theta}_k^-)}{\partial \mathbf{x}_k}\Big|_{\mathbf{x}=\hat{\mathbf{x}}_k^-}$,

$\mathbf{A}_{k-1} = \frac{\partial f(\mathbf{x}_{k-1}, u_{k-1}, \hat{\theta}_k^-)}{\partial \mathbf{x}_{k-1}}\Big|_{\mathbf{x}=\hat{\mathbf{x}}_{k-1}^+}$

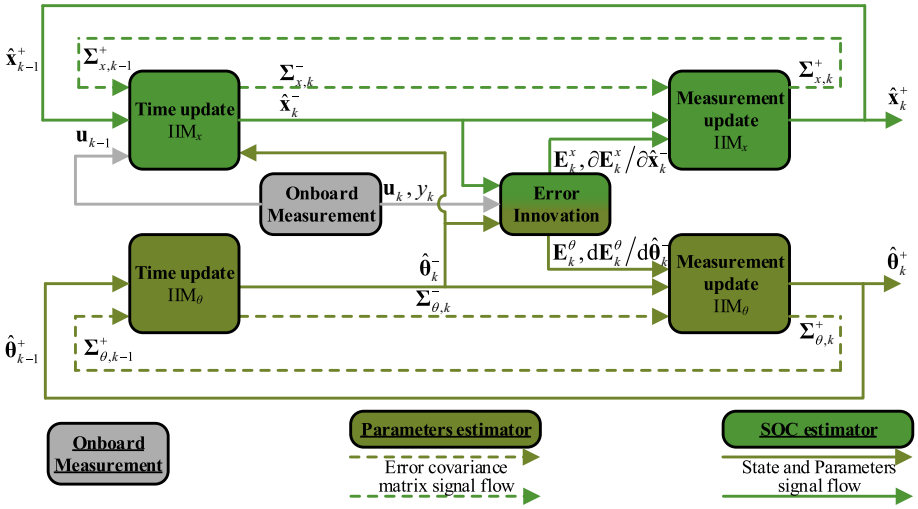

Fig. 7. The flowchart of the online state and parameters estimator based dual IIM algorithm.

$$\frac{d\hat{\mathbf{x}}_{k-1}^{+}}{d\boldsymbol{\theta}} = \frac{d\hat{\mathbf{x}}_{k-1}^{-}}{d\boldsymbol{\theta}} - \mathbf{L}_{k-1}^{x}\frac{dg(\hat{\mathbf{x}}_{k-1}^{-}, u_{k-1}, \boldsymbol{\theta})}{d\boldsymbol{\theta}} \tag{30}$$

where $\mathbf{L}_{k-1}^{x} = \boldsymbol{\Sigma}_{x,k-1}^{-}\left[\mathbf{I} + (\mathbf{C}_{k-1}^{x})^{T}\boldsymbol{\Sigma}_{v}^{-1}\mathbf{C}_{k-1}^{x}\boldsymbol{\Sigma}_{x,k-1}^{-}\right]^{-1}(\mathbf{C}_{k-1}^{x})^{T}\boldsymbol{\Sigma}_{v}^{-1}$. It is not a function of $\boldsymbol{\theta}$. $\partial g(\hat{\mathbf{x}}_{k}^{-}, u_k, \boldsymbol{\theta})/\partial\boldsymbol{\theta}$ and $\partial f(\hat{\mathbf{x}}_{k-1}^{+}, u_{k-1}, \boldsymbol{\theta})/\partial\boldsymbol{\theta}$ can be expressed as follows:

$$\begin{cases} \frac{\partial g(\hat{\mathbf{x}}_{k}^{-}, u_k, \boldsymbol{\theta})}{\partial\boldsymbol{\theta}} = \begin{bmatrix} -I_{L,k}^{+} & -I_{L,k}^{-} & 0 & 0 & 0 & 0 & 0 \end{bmatrix} \\ \frac{\partial f(\hat{\mathbf{x}}_{k-1}^{+}, u_{k-1}, \boldsymbol{\theta})}{\partial\boldsymbol{\theta}} = \begin{pmatrix} 0 & 0 & 0 & 0 & 0 & 0 & 0 \\ 0 & 0 & U_{1,k-1} & 0 & (1-\alpha_1)I_{L,k-1} & 0 & 0 \\ 0 & 0 & 0 & U_{2,k-1} & 0 & (1-\alpha_2)I_{L,k-1} & 0 \\ 0 & 0 & 0 & 0 & 0 & 0 & (U_{H,k-1} - M(z_{k-1}, \dot{z}))\frac{-|I_{L,k-1}|\Delta t}{C_N}\Gamma_{k-1} \end{pmatrix} \end{cases} \tag{31}$$

5. Verification and discussion

The proposed algorithm is verified under two validation experimental conditions, including (1) constant current (1C), (2) dynamic current. Here, the DST (dynamic stress test) loading profile according to USABC is used to evaluate the performance of a battery model and SOC estimation method. The experimental current and calculated SOC profiles of the $LiFePO_4$ cell are shown in Fig. 8, where the cell has been fully charged with constant current and constant voltage protocol, thus the initial SOC is 100%. Fig. 8(a) is the current profile of one DST cycle, Fig. 8(b) is the SOC reference trajectory profile of the entire DST. It should be noted that, in all cases, SOC reference profiles are calculated by using ampere hour counting on measured data. The robustness of the proposed method is verified by comparing the performance of the EKF and UKF methods on both constant current and dynamic current conditions. Values of the battery model parameters of the dual-IIM algorithm are identified on-line, while values of the battery model parameters of the EKF and UKF methods are calculated off-line according to the experimental results listed in Section 2.

Furthermore, in order to evaluate the hysteresis model, pulse current test scheme, in which SOC is varied over a preset loop, as shown in Fig. 9, has been implemented on IFP1865140-type batteries.

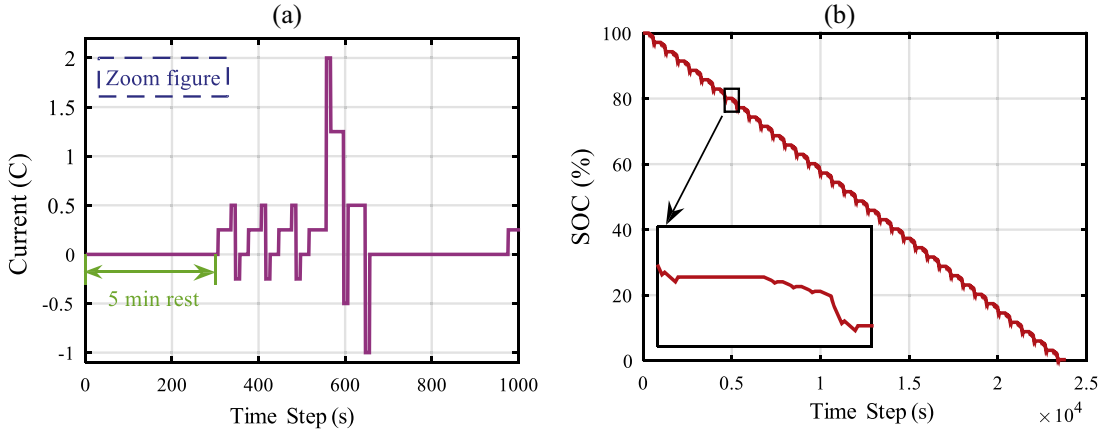

Fig. 8. Plots showing current vs. time and SOC vs. time for DST test. (a) Current for one DST cycle, and (b) the SOC reference trajectory.

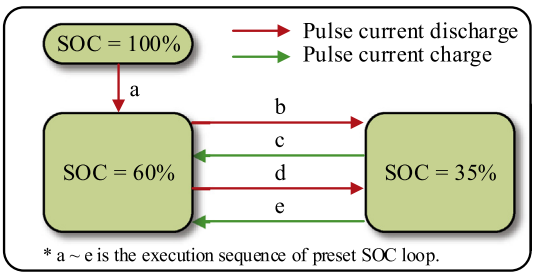

Fig. 9. SOC loops obtained through the current pulses to verify the modified hysteresis model.

5.1. Under constant current condition

In order to verify the performance of the dual IIM algorithm based estimator under constant current. The battery is discharged with a constant rate 1C. The online estimation results of the proposed estimator and the estimation results of the EKF and UKF methods are plotted in Figs. 10 and 11. The numeric results are shown in Table 3. The SOC estimation results and estimation errors are plotted in Fig. 10(a) and (b), while the estimated voltages and estimation errors are plotted in Fig. 11(a) and (b). Fig. 10(c) presents the estimated hysteresis constant γ based on the dual IIM algorithm. The RMSEs of the estimated SOC based on the EKF and UKF methods are 2.64% and 1.78%, respectively, while the RMSE of the estimated SOC based on the proposed method is 1.70%. The RMSEs of the estimated voltages based on EKF and UKF are 35.9 mV and 39.2 mV, respectively, while the RMSE of estimated voltage based on the proposed method is 9.72 mV. The MaxAEs of the estimated SOC based on the EKF and UKF methods are 4.39% and 1.77%, respectively, while the MaxAE of the estimated SOC based on the proposed method is 1.51%. The MaxAEs of the estimated voltages based on the EKF and UKF are 129.8 mV and 129.5 mV, respectively, while the MaxAE of the estimated voltage based on the proposed method is 71.0 mV (2% of its upper cutoff voltage). As can be seen in Fig. 10(b) and (c), the estimation value based on the proposed IIM-based estimator converges to real SOC with an error of $\pm 2\%$, and the estimated hysteresis γ converge to 10.08. These results show that the proposed method provides higher accuracy for estimating SOC and the terminal voltage of the battery than the EKF and UKF methods under constant current condition. What is more, the values of battery parameters are updated online based on the dual-IIM algorithm. Therefore, the proposed method can provide better robustness to suppress the system parameter perturbations.

5.2. Under dynamic current condition

In order to further verify the robustness performance of the dual IIM algorithm based estimator under dynamic current condition. The battery is discharged with a DST loading profile. The online estimation results of the proposed estimator and the estimation results of the EKF and UKF methods are plotted in Figs. 12 and 13. The numeric results are shown in Table 3. The SOC estimation results and estimation errors are plotted in Fig. 12(a) and (b), while the estimated voltages and estimation errors are plotted in Fig. 13(a)–(c). Fig. 12(c) presents the estimated hysteresis constant γ based on the dual IIM algorithm. The RMSEs of the estimated SOC based on the EKF and UKF methods are 3.03% and 2.09%, respectively, while the RMSE of the estimated SOC based on the proposed method is 1.68%. The RMSEs of the estimated voltages based on the EKF and UKF are 23.3 mV and 23.7 mV, respectively, while the RMSE of the estimated voltage based on the proposed method is 17.9 mV. The MaxAEs of the estimated SOC based on the EKF and

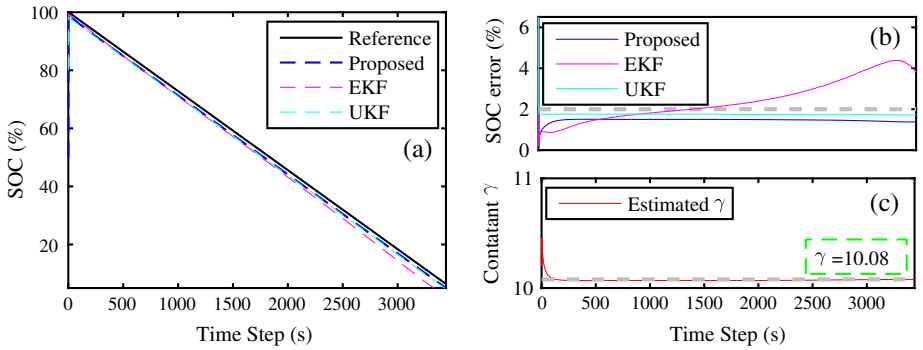

Fig. 10. SOC estimation results under constant current condition: (a) SOC; (b) SOC error; and (c) hysteresis constant γ.

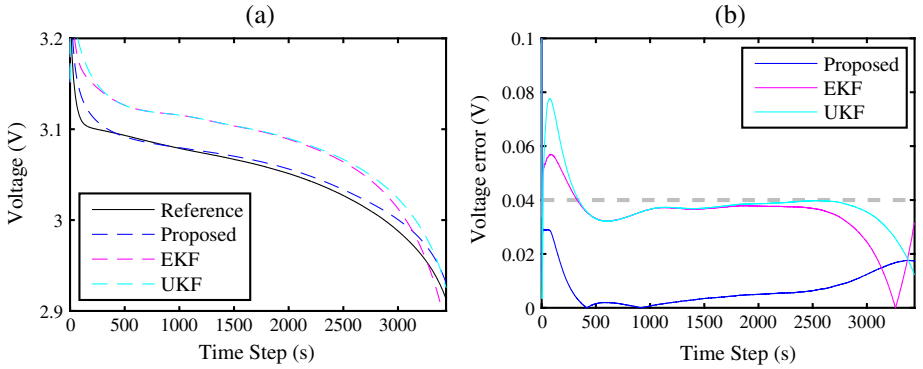

Fig. 11. Voltage estimation results under constant current condition: (a) voltage; and (b) voltage error.

Table 3
Performance of dual-IIM based SOC online estimator.

Conditions	γ	MaxAE[a]						RMSE[b]					
		SOC (%)			Voltage (mV)			SOC (%)			Voltage (mV)		
		IIM	EKF	UKF	IIM	EKF	UKF	IIM	EKF	UKF	IIM	EKF	UKF
Constant current	10.08	1.51	4.39	1.77	71.0	129.8	129.5	1.70	2.64	1.78	9.72	35.8	39.2
Dynamic current	10.58	2.10	4.53	2.25	193.6	98.3	83.9	1.68	3.03	2.09	17.9	23.3	23.7

[a] MaxAE = Maximum Absolute Error.
[b] RMSE = Root Mean Square Error.

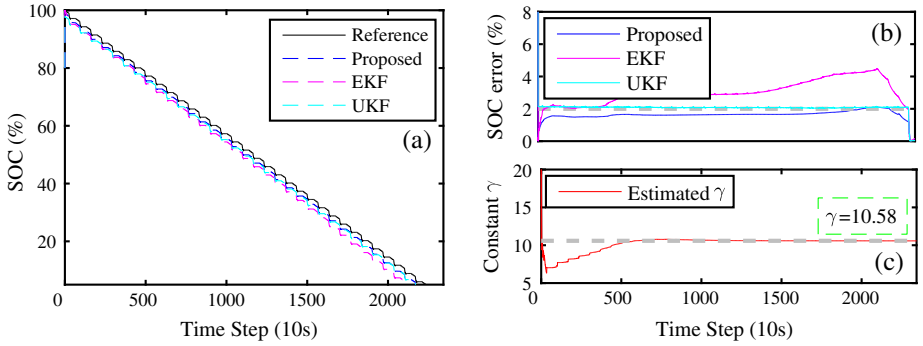

Fig. 12. SOC estimation results under dynamic current condition: (a) SOC; (b) SOC error; and (c) hysteresis constant γ.

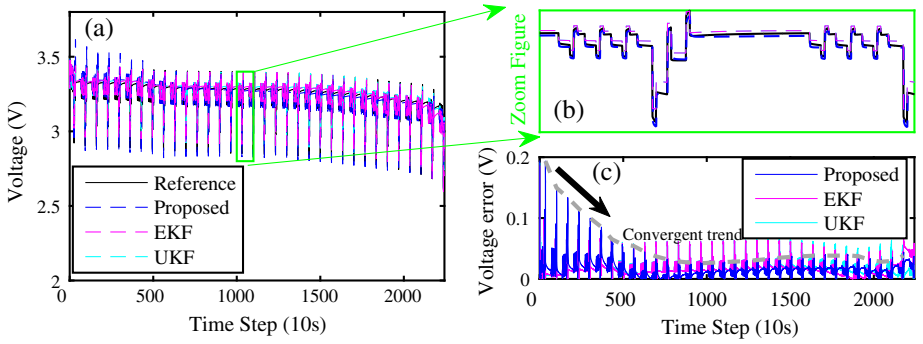

Fig. 13. Voltage results under constant dynamic condition: (a) voltage; (b) zoom figure; and (c) voltage error.

UKF methods are 4.53% and 2.25%, respectively, while the MaxAE of the estimated SOC based on the proposed method is 2.10%. The MaxAEs of the estimated voltages based on EKF and UKF are 98.3 mV and 83.9 mV, respectively, while the MaxAE of the estimated voltage based on the proposed method is 193.6 mV (5.3% of its upper cutoff voltage). As can be seen in Fig. 12(b) and (c), the estimation value based on the proposed IIM-based estimator converges to real SOC with an error of $\pm 2\%$ and the estimated hysteresis γ converge to 10.08. Additionally, according to Fig. 13(c), it can be seen the voltage error based on the proposed method shows a convergent trend. These results show that the proposed method also provides accurate online estimation for estimating SOC and

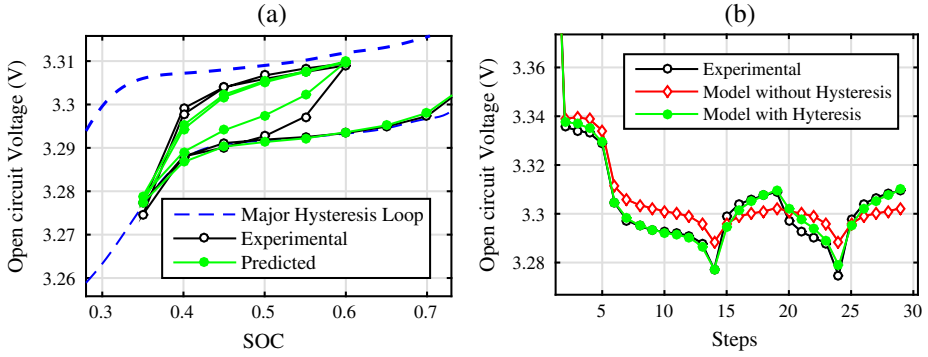

Fig. 14. Comparison of the measured and predicted OCV: (a) with respect to cell SOC, and (b) fictitious evolution.

terminal voltage of battery under dynamic current condition. Therefore, the proposed method has shown great robustness under different current conditions.

5.3. Verification of hysteresis model

To verify accuracy of the hysteresis model, pulse current test scheme, as shown in Fig. 9, has been implemented on IFP1865140-type batteries. The results are plotted in Fig. 14. Fig. 14(a) shows the results in the SOC–OCV plane for the preset SOC loop. The results are also presented in Fig. 14(b) as a fictitious time evolution of the OCV, where the voltage values are determined every SOC step. Both experimental and predicted data are reported. From Fig. 14 it can be noted that the excellent agreement between the experimental and the model data which contains a hysteresis voltage state. The overall RMSE is 8.7 mV. By contrast, the experimental values have a significant deviation with the model output, which has not considered the hysteresis voltage. The overall RMSE is 13.2%. The important result obtained is that the hysteresis model provides a better capability of reproducing the experimental results for a cell.

Based on the above different validation experiments, it can be concluded that the dual IIM based SOC estimator works well against uncertain operating currents. It can also suppress the measurement noises and provide better performance for SOC estimation. Meanwhile, the uncertainty battery model and its parameters can be updated online through the IIM method. What is more, the accurate OCV hysteresis can be predicted online, which is helpful for reliable and accurate battery SOC estimation.

6. Conclusion

SOC of a Lithium-ion battery is an important evaluation index in BMS for electric vehicles and smart grids. However, the existing special open-circuit-voltage characteristics of $LiFePO_4$ batteries complicate the estimation of SOC. To obtain accurate and reliable estimation, the main contributions of this work can be summarized as following for items. Firstly, in considering of the OCV hysteresis phenomena, an equivalent circuit battery model that include the component describing hysteresis characteristic is introduced. Secondly, because sensor noises of the measurement system are inevitable, it is hard to accurately quantify the model parameters with the measured data. To establish an online parameter and state joint estimator, this work has developed an online dual IIM algorithm for SOC and voltage of the battery, where one IIM is employed to develop an online parameter identification method through the real-time the measurements of the battery currents and voltages, while the other IIM algorithm is applied to establish the estimator for battery SOC. Finally, the proposed method has been verified by a $LiFePO_4$ battery cell under different operating current conditions. The experimental results indicate that the estimation value based on the proposed IIM-based estimator converges to real state-of-charge with an error of $\pm 2\%$, and the battery model can simulates OCV hysteresis phenomena robustly with high accuracy.

Acknowledgement

This work was supported by the National Natural Science Fund of China (Grant No. 61375079).

References

[1] Wang L, Cheng Y, Zhao X. A $LiFePO_4$ battery pack capacity estimation approach considering in-parallel cell safety in electric vehicles. Appl Energy 2015;142:293–302.
[2] Liu X, Wu J, Zhang C, Chen Z. A method for state of energy estimation of lithium-ion batteries at dynamic currents and temperatures. J Power Sources 2014;270:151–7.
[3] Baronti F, Zamboni W, Femia N, Roncella R, Saletti R. Experimental analysis of open-circuit voltage hysteresis in lithium–iron–phosphate batteries. IN: Industrial electronics society, IECON 2013–39th annual conference of the IEEE2013. p. 6728–33.
[4] Ng KS, Moo C-S, Chen Y-P, Hsieh Y-C. Enhanced coulomb counting method for estimating state-of-charge and state-of-health of lithium-ion batteries. Appl Energy 2009;86:1506–11.
[5] Yang N, Zhang X, Li G. State of charge estimation for pulse discharge of a $LiFePO_4$ battery by a revised Ah counting. Electrochim Acta 2015;151:63–71.
[6] Zhong L, Zhang C, He Y, Chen Z. A method for the estimation of the battery pack state of charge based on in-pack cells uniformity analysis. Appl Energy 2014;113:558–64.
[7] Liu XT, Liu XT, He Y, Chen ZH. Based-V_{min}-EKF SOC estimation for power Li-ion battery pack. Kongzhi yu Juece/Control and Decision 2010;25:445–8.
[8] Zhang W, Shi W, Ma Z. Adaptive unscented Kalman filter based state of energy and power capability estimation approach for lithium-ion battery. J Power Sources 2015;289:50–62.
[9] Wang Y, Zhang C, Chen Z. A method for state-of-charge estimation of $LiFePO_4$ batteries at dynamic currents and temperatures using particle filter. J Power Sources 2015;279:306–11.
[10] He Y, Liu X, Zhang C, Chen Z. A new model for state-of-charge (SOC) estimation for high-power Li-ion batteries. Appl Energy 2013;101:808–14.
[11] Charkhgard M, Farrokhi M. State-of-charge estimation for lithium-ion batteries using neural networks and EKF. Ind Electron, IEEE Trans 2010;57:4178–87.
[12] Plett GL. Extended Kalman filtering for battery management systems of LiPB-based HEV battery packs: Part 3. State and parameter estimation. J Power Sources 2004;134:277–92.
[13] Xiong R, Sun F, He H, Nguyen TD. A data-driven adaptive state of charge and power capability joint estimator of lithium-ion polymer battery used in electric vehicles. Energy 2013;63:295–308.
[14] Liu X, Chen Z, Zhang C, Wu J. A novel temperature-compensated model for power Li-ion batteries with dual-particle-filter state of charge estimation. Appl Energy 2014;123:263–72.
[15] Dreyer W, Jamnik J, Guhlke C, Huth R, Moškon J, Gaberšček M. The thermodynamic origin of hysteresis in insertion batteries. Nat Mater 2010;9:448–53.
[16] Roscher MA, Bohlen O, Vetter J. OCV hysteresis in Li-ion batteries including two-phase transition materials. Int J Electrochem 2011;2011:1–6.
[17] Roscher MA, Sauer DU. Dynamic electric behavior and open-circuit-voltage modeling of $LiFePO_4$-based lithium ion secondary batteries. J Power Sources 2011;196:331–6.
[18] Sasaki T, Ukyo Y, Novák P. Memory effect in a lithium-ion battery. Nat Mater 2013;12:569–75.
[19] Plett GL. Extended Kalman filtering for battery management systems of LiPB-based HEV battery packs: Part 2. Modeling and identification. J Power Sources 2004;134:262–76.
[20] Kim J, Lee S, Cho B. The state of charge estimation employing empirical parameters measurements for various temperatures. IEEE Int Power Electr 2009:1567–72.
[21] Petzl M, Danzer MA. Advancements in OCV measurement and analysis for lithium-ion batteries. Energy Convers, IEEE Trans 2013;28:675–81.
[22] Sridhar DDaR. Sequential estimation of states and parameters in noisy nonlinear dynamical systems. J Fluids Eng 1966;88:362–8.
[23] Akin-Bohner E, Atici FM. A quasilinearization approach for two point nonlinear boundary value problems on time scales. Rocky Mt J Math 2005;35:19–45.